IOP Conf. Series: Materials Science and Engineering **373** (2018) 012016 doi:10.1088/1757-899X/373/1/012016

Influence of the welding temperature and the welding speed on the mechanical properties of friction stir welds in EN AW-2219-T87

A Bachmann, M Krutzlinger and M F Zaeh

Institute for Machine Tools and Industrial Management, Technical University of Munich, Boltzmannstrasse 15, 85748 Garching, Germany

Abstract. Friction Stir Welding (FSW) is an innovative joining technique, which has proven to produce high quality joints in high strength aluminum alloys. Consequently, it is commonly used to manufacture lightweight aerospace structures with stringent requirements. For these structures, it is necessary to ensure a high ultimate tensile strength (UTS). Various studies have reported that the UTS is significantly influenced by the welding parameters. Samples welded with different parameter sets showed a considerably different UTS, despite being free from detectable welding defects (e.g. tunnel defect, voids, or lack of penetration). Based on the observations in the literature, a hypothesis was posed. The welding temperature along with the welding speed determine the UTS of the weld. This study aims to prove this hypothesis experimentally by using temperature-controlled FSW to join plates of EN AW-2219-T87 in butt joint configuration. The welded samples were examined using visual inspection, metallography, X-ray imaging, and uniaxial tensile tests. Finally, a statistical analysis was conducted. Hereby, the hypothesis was confirmed.

1. Introduction

The use of aluminum alloys has significantly grown in the second half of the 20th century. This was mainly driven by the density of aluminum, which is relatively low compared to other engineering materials, such as steel [1]. The aerospace industry employs high strength aluminum alloys in order to reduce the structural mass of airplanes and rockets. However, one major drawback of these lightweight materials is their limited fusion weldability. When high-strength aluminum alloys are welded, they tend to the formation of pores and hot cracks, both of which are typical for fusion-welding processes. Friction Stir Welding (FSW) is an innovative solid-state joining process that was invented in 1991. Since the solidus temperature of the material is usually not exceeded during FSW, the formation of hot cracks and pores can be avoided. For this reason, FSW has quickly evolved as a key joining process in the aerospace industry [2]. An important example of a high-strength aluminum alloy that is employed for rocket structures is EN AW-2219-T87 [3]. It contains a high amount of copper (approximately 6 %), which yields advantageous mechanical properties by precipitation hardening. However, the weld seam remains the weakest element of structures made of EN AW-2219-T87. In order to enable the next steps of mass reduction, it is crucial to understand and control the mechanisms that deteriorate the mechanical properties of friction stir welds in EN AW-2219-T87.

The micro structure of friction-stir-welded and arc welded samples of EN AW-2219-T851 was compared by CAO & KOU. They observed the formation of an eutectic phase in the arc welded samples,

which was probably formed due to melting and subsequent solidification. In the friction stir welds, θ-phase particles (Al_2Cu) were found in the welding nugget (WN), but no evidence of bulk melting could be determined. However, large clusters of θ-particles appeared towards the end of the weld and in the vicinity of the probe tip. This led to the conclusion that the formation of the particle clusters is associated to the material flow around the probe [4].

ELANGOVAN & BALASUBRAMANIEN investigated the influence of the geometrical features of the probe and the rotational speed on the mechanical properties. The best results were obtained with a square probe and a rotational speed of 1600 min^{-1}. The superiority of the square probe was confirmed in a second study, in which the shape of the probe and the welding speed were varied [5; 6].

The corrosion behavior of friction stir welded EN AW-2219-T87 samples was investigated by SUREKHA ET AL. and SRINIVASAN ET AL. A dependency of the corrosion resistance from the rotational speed and the welding speed was observed. It was assumed that the effect was caused by the dissolution of copper precipitates [7]. Furthermore, a higher corrosion resistance of the welding zone compared to the base material was reported [8].

The microstructure of a friction-stir-welded EN AW-2219-T87 sample was analyzed by ARORA ET AL. In the welding nugget, a grain refinement was observed along with a 40 % dissolution of the θ-particles. It was assumed that both are caused by dynamic recrystallization. The dissolution of θ-particles was also observed in the thermomechanically affected zone (TMAZ), although it was not as significant as in the WN. Furthermore, it was reported that grain coarsening occurred in the TMAZ [9].

A superior ultimate tensile strength (UTS) and less variance in the UTS of friction stir welds compared to arc welds in EN AW-2219-T87 were reported by KAHNERT ET AL. The tensile tests were conducted under cryogenic conditions (20 K – 77 K), which mirrors the environment in rocket fuel tanks [3].

The influence of the rotational speed on the mechanical properties of friction-stir-welded EN AW-2219-T87 samples was investigated by SCHNEIDER ET AL. It was observed that an increased rotational speed leads to an increased UTS and hardness of the welds. The authors concluded that the increased rotational speed supports the dissolution of θ-particles and the coarsening of θ'-particles [10].

DOUDE ET AL. investigated the influence of the rotational speed and the welding speed on the mechanical properties of friction-stir-welded EN AW-2219-T87 samples. A parameter window for defect-free friction stir welds was identified. Within the parameter window, an increased rotational speed increased the UTS as well as the hardness of the weld. As the rotational speed mainly influences the welding temperature, it was assumed that the welding temperature governs the metallurgical effects. It was concluded that during FSW of heat-treatable aluminum-copper alloys, the welding temperature has to be sufficient to enable the dissolution of the θ-particles and to prevent their coarsening [11].

A similar conclusion was made by RAO ET AL., who investigated the influence of the tool geometry on the UTS of friction-stir-welded EN AW-2219-T87 samples. The highest UTS was achieved using a hexagonal probe, which also led to the highest welding temperature [12].

A thorough investigation on the formation and the behavior of copper precipitates during FSW of EN AW-2219-T87 was conducted by KANG ET AL. It was observed that the θ'- and θ''-particles are fully dissolved in the WN, whereas θ-particles are only partially dissolved. In the heat affected zone (HAZ), the θ''-particles were also dissolved completely, whereas θ'-particles were only dissolved partially. This effect was explained by the decreasing temperature perpendicular to the welding direction. It was assumed that this effect is also the reason for the varying hardness values measured in this direction. As reported by CAO & KOU, large clusters of θ-particles were detected in the WN. From the analysis of the microstructure it was concluded that diffusion processes are not responsible for the formation of the particle clusters. It was assumed that their formation is associated to the material flow around the probe. However, tensile tests of the welded samples showed no impact of the particle clusters on the mechanical properties [13; 14].

To summarize, the welding temperature and the welding speed are believed to be the determining factors for the mechanical properties of the welds. Both parameters influence the diffusion processes during and immediately after welding. This assumption has been supported by the results obtained from the analysis of the microstructure. However, it has not been proven that constant mechanical properties can be ensured by welding with different tools at the same welding temperatures. Furthermore, the correlation between welding temperature, welding speed, and resulting UTS is unknown.

2. Hypotheses and methodology

2.1. Hypotheses

Related works have suggested that the dissolution and coarsening of copper precipitants determines the mechanical properties of friction stir welds in EN AW-2219-T87. The dissolution as well as the coarsening of precipitants are mainly driven by time- and temperature-dependent processes. Hence, the thermal cycle during FSW has to be controlled in order to regulate the mechanical properties of the weld. The scope of this paper is to prove that this can be achieved by temperature-controlled FSW. The subsequent hypotheses, which have yet to be proven, are:

- The welding temperature and the welding speed have a significant influence on the mechanical properties of friction stir welds. Therefore, a parameter set composed by a welding temperature and a welding speed can be transferred to a different welding task resulting in a similar UTS.
- The tool rotation serves to induce the required heat energy and to ensure the necessary material flow during FSW. It is supposed that a rotational speed ensuring a suitable welding temperature provides also an adequate material flow. Hence, it is admissible to regulate the welding temperature by adjusting the rotational speed.

2.2. Approach

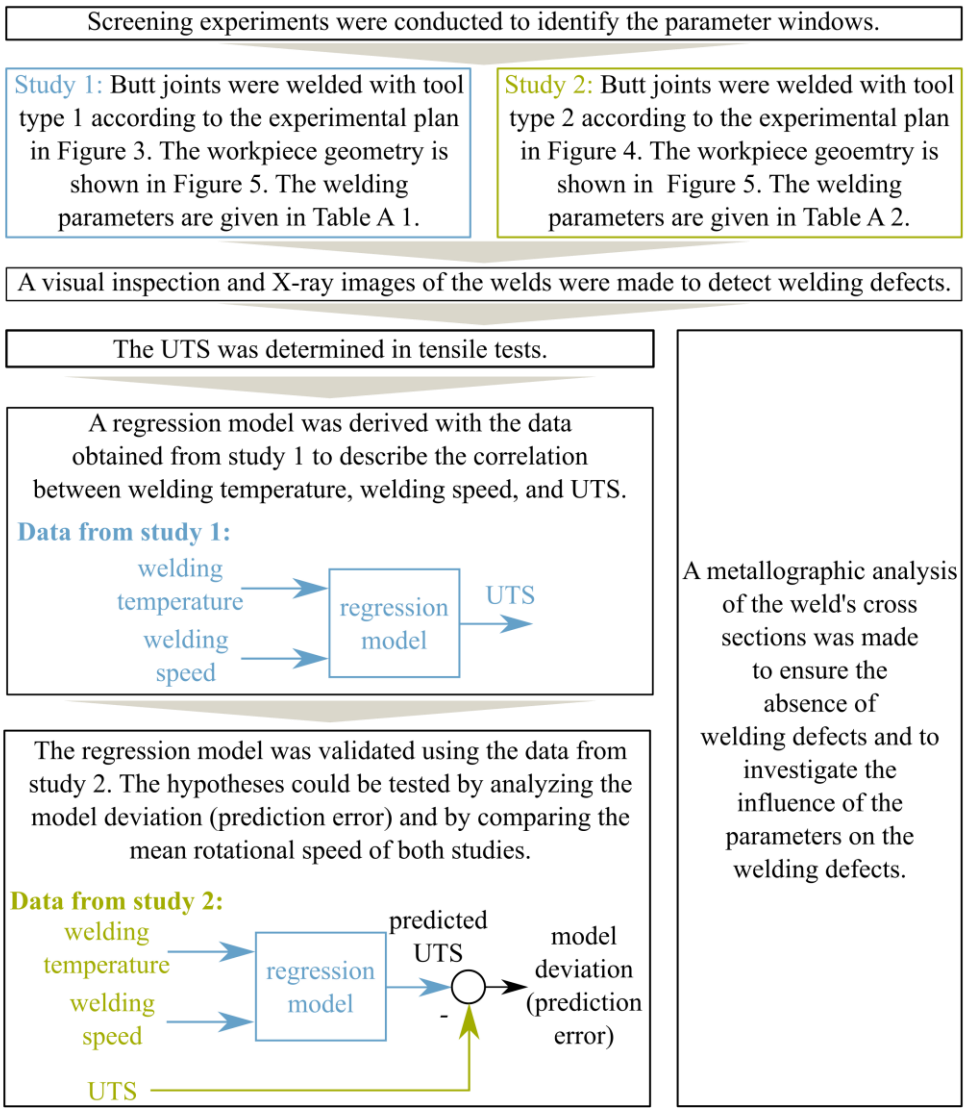

Figure 1. Experimental set-up to corroborate the hypotheses posed in section 2.1

Two sequential parameter studies (study 1 and study 2) were conducted to corroborate the hypotheses posed in section 2.1. The welding speed and the welding temperature were varied in both studies. The temperature control system presented in BACHMANN ET AL. [15] was used to control the welding temperature. Two tools of the same geometry, but with different dimensions were used during each study. Thereby, it was ensured that similar welding temperatures were caused by significantly different rotational speeds. The results of the parameter study 1 were used to identify a regression model, which describes the correlation between the welding temperature, the welding speed and the UTS. The data from parameter study 2 were employed to both the validation of the model and the verification of the hypotheses. The complete experimental procedure is depicted in Figure 1.
First, the parameter windows for the tools were identified in preliminary screening trials. Subsequently, the actual welding experiments were conducted according to an experimental plan. The welded plates were inspected visually and X-rayed to reveal volumetric defects in the welds. Thereby, an influence of detectable welding defects (e.g. voids, tunnel defects, or lack of penetration) on the resulting UTS could be avoided. The plates that passed the non-destructive testing (NDT) were selected to extract specimens for the uniaxial tensile tests and for metallography. Finally, the UTS and the input parameters were used to derive a regression model, which was employed to predict the UTS for the study 2. The model was deemed to be valid if the residuals and the prediction error were within the same order of magnitude. This corroborates the hypothesis, because it is expected that the different tool sizes result in significantly different rotational speeds to provide the same temperatures. The different methods and the equipment used for each step of the experimental procedure are described in the following.

2.2.1. Experimental set-up and screening. The welding machine used during the studies is based on an industrial robot. It is described and depicted in BACHMANN ET AL. [15]. Furthermore, the temperature control system described by BACHMANN ET AL. [15] was used throughout the studies for this paper. The temperature measuring system was described by COSTANZI ET AL. [16]. Two tools of the same geometry but of different sizes were employed in this study. The tool geometries and their dimensions are given in Figure 2 and Table 1.

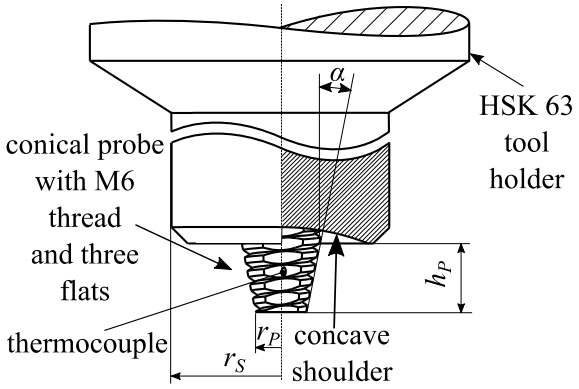

Figure 2. Tool geometry with the most important dimensions of the FSW tools used in the experiments [15]

Preliminary screening experiments were conducted to find a suitable downward force F_z as well as to determine the parameter window, in which macroscopic welding defects do not occur. Hereby, bead-on-plate welds were made on 4 mm thick plates of EN AW-2219-T87. The welds were inspected visually and a bending test was conducted to ensure full penetration of the plates. Cross-sections of the welds were extracted to verify the absence of tunnel defects. The resulting parameter windows are depicted in Figure 3 for tool type 1 and Figure 4 for tool type 2, respectively. The parameter window for tool type 1 extends to a welding speed of v_S = 400 mm/min. The maximum welding temperature was set to $T_{S,max}$ = 540 °C, which is beneath the solidus temperature $T_{solidus}$ = 548 °C of EN AW-2219-T87 [1]. The minimum welding temperature was determined in the screening experiments. It marks the limit to the onset of lack of consolidation or tunnel defects. The maximum rotational speed of the spindle was 3000 min^{-1}. This led to the limitations in parameter window 2 (see Figure 4). Due to the smaller tool diameter, higher rotational speeds were required by the temperature controller than could be provided

by the spindle motor. The suitable downward force for tool type 1 was to F_z = 9000 N. Thereby, welds with little flash and without surface lack of fill could be produced. The screening experiments with tool type 2 showed similar results for equal welding temperatures and welding speeds using a downward force of F_z = 7000 N.

Table 1. Numerical values of the tool dimensions (see Figure 2)

	Probe radius r_P in mm	Shoulder radius r_P in mm	Conical probe angle α in °	Probe length h_P in mm
Tool type 1	2.350	10	11	3.87
Tool type 2	1.835	8	10	4.15

2.2.2. Welding experiments. Two parameter studies labeled study 1 and study 2 were conducted. In both studies the welding temperature and the welding speed were varied systematically, the tilt angle of the tool was kept constant at 2.5° throughout the experiments. The geometry of the samples, which were welded in butt joint configuration, is shown in Figure 5. The faying surfaces of the plates were cleaned thoroughly with isopropanol before welding. A rigid clamping device was used to avoid gaps between the joining partners. The weld length on each plate was 450 mm. In order to reduce the experimental effort, the welding temperature was changed in the middle of the weld (see Figure 5). The temperature was changed (transition zone) over a distance of 55 mm in the center of the weld. This part was not used for further investigation.

Tool type 1 was employed for study 1. More heat could be delivered to the process zone due to the larger diameters of the shoulder and of the probe. Consequently, higher welding temperatures could be achieved even at increased welding speeds. The parameter window is depicted in Figure 3. A modified D-optimal experimental plan was used due to the restrictions posed by the arising welding defects at high welding speeds and low welding temperatures. The parameter sets, which were tested in study 1, are depicted as circles in Figure 3. The trials using the center point as well as two random points were repeated to determine the reproducibility of the results of the welding experiments.

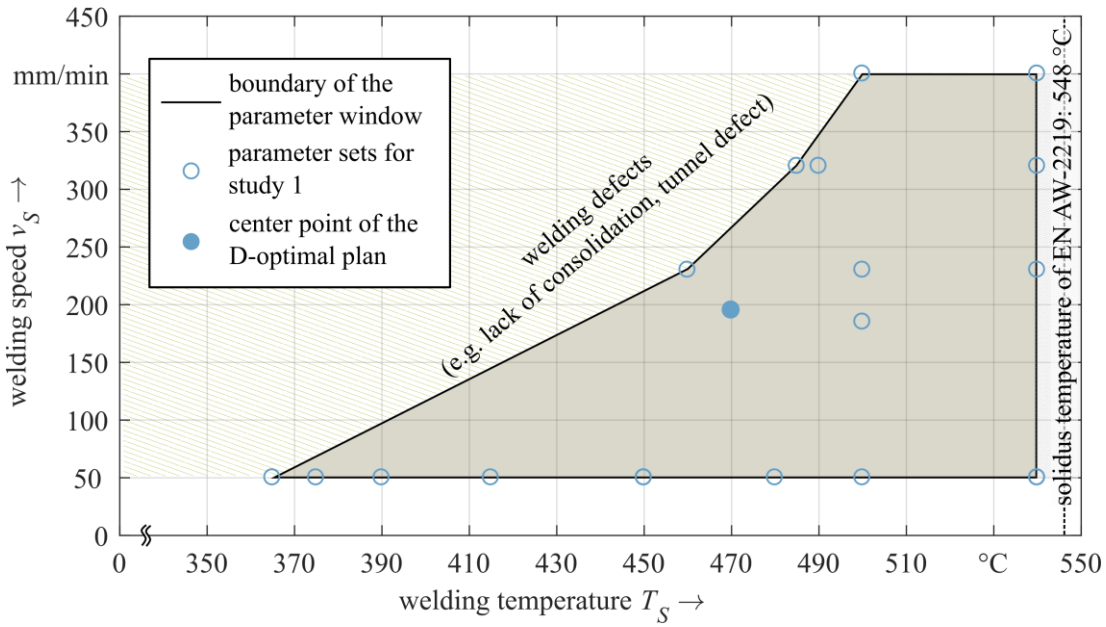

Figure 3. Parameter window 1 and parameter sets for the study 1

Tool type number 2 was employed during study 2. Owing to the smaller shoulder and probe diameter, the amount of heat produced with tool type 2 was significantly lower. This led to further restrictions of the parameter window, because the rotational speed required from the controller was higher than the maximum rotational speed provided by the spindle. This limitation arising from the welding machine is marked in Figure 4. As a consequence, the parameter window 2 was split and three experimental plans

were derived: Two D-optimal plans covered the parameter window at high and low temperature levels and a full factorial plan was used for the intermediate temperature levels. The parameter window for the study 2 and its division into the three experimental plans is shown in Figure 4. The parameter sets from study 2 are marked as green asterisks. The center point of the full factorial sub plan (marked as dashed asterisk in Figure 4) was repeated twice to assess the reproducibility of the welding process.

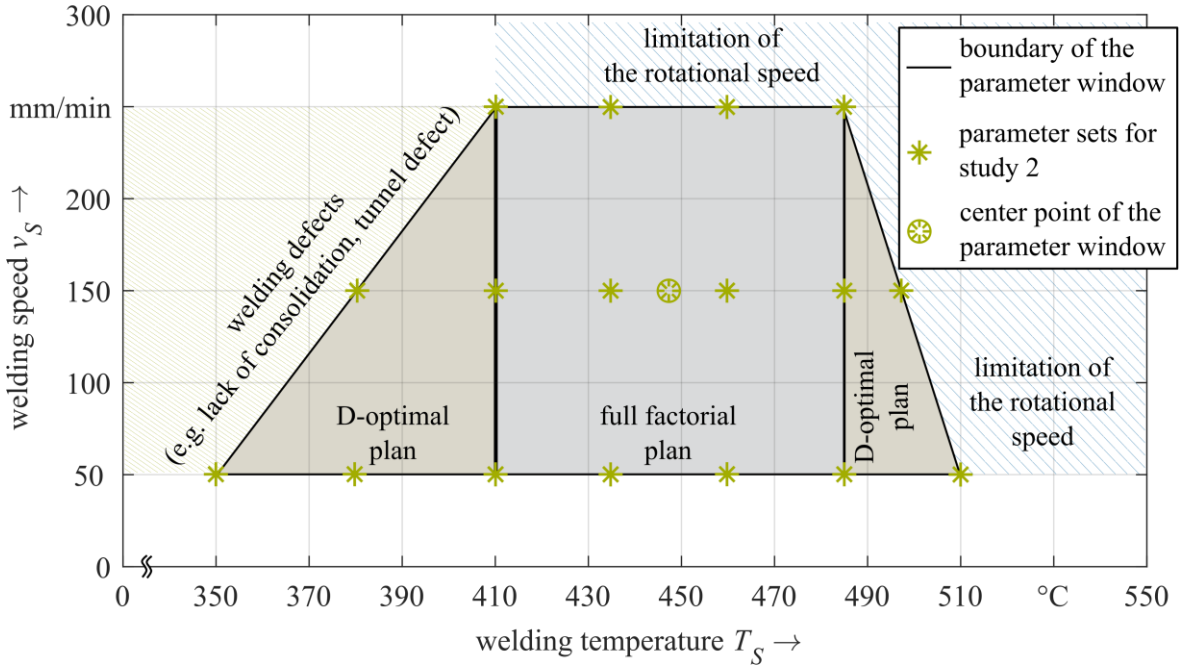

Figure 4. Parameter window 2 and parameter sets for the study 2

2.2.3. Visual inspection. The welds were inspected visually by employing a criteria set. The primary focal points were: surface appearance (regular surface, surface galling), regularity of the width, flash formation, surface cracks, appearance of the weld root (suck back or excessive convexity), and appearance of the key hole. Tunnel defects can often be identified by inspecting the keyhole, as the tunnel often evolves up to the lateral surface of the key hole.

2.2.4. X-ray imaging. The welded plates were examined using X-ray attenuation imaging. Zones containing abnormalities in the X-ray image were marked on the plates. These areas were not used for the subsequent analysis to avoid that the macroscopic welding defects influence the results.

2.2.5. Tensile tests. The tensile tests were conducted approximately six weeks after welding. It was assumed that potential post-weld aging was terminated after this period. The specimens required for the tensile tests were extracted from the welded plates as shown in Figure 5. The positions of the specimens were selected according to the restrictions given by DIN EN ISO 25239-3. One plate was used to investigate two parameter sets, as the parameters were changed in the center of the weld. The width of the sheets differed to facilitate the accessibility of the robot and to enable an adequate clamping.

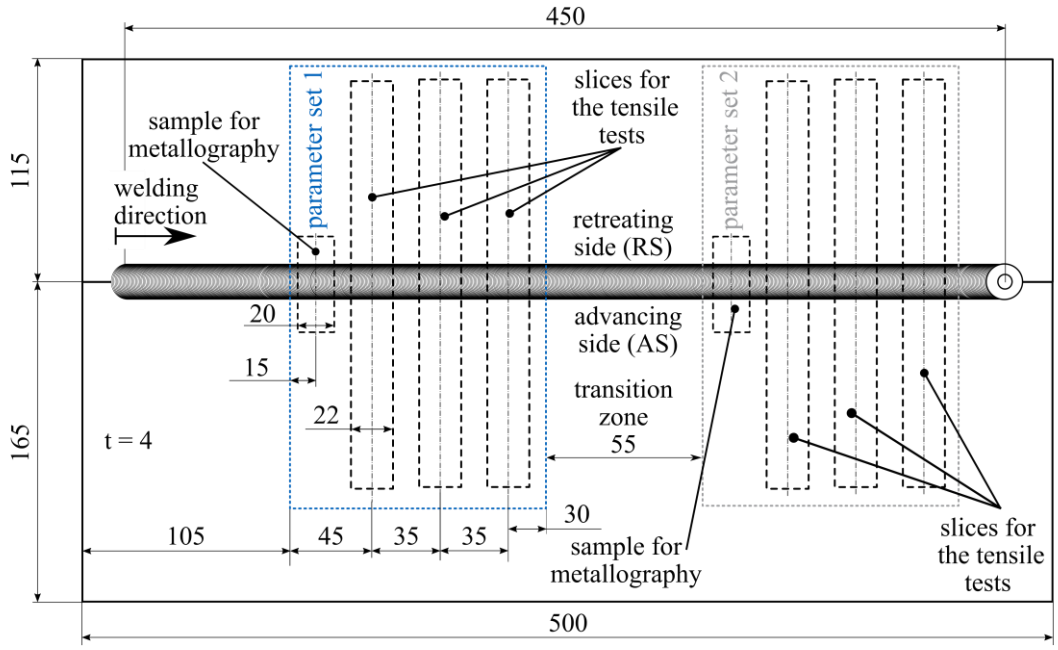

Figure 5. Dimensions of the welded plates with the position of the specimens for the tensile test and the samples for metallography in mm

Three samples were extracted for each parameter set to enable the estimation of the process variance. The slices obtained from the plate were milled to the final specimen geometry shown in Figure 6. The specimen geometry was adapted from the shape E in DIN 50125. Hereby, the length and the width of the specimen were increased to avoid slipping during the tensile test. The uniaxial tensile tests were performed according to the guidelines in DIN EN ISO 6892-1.

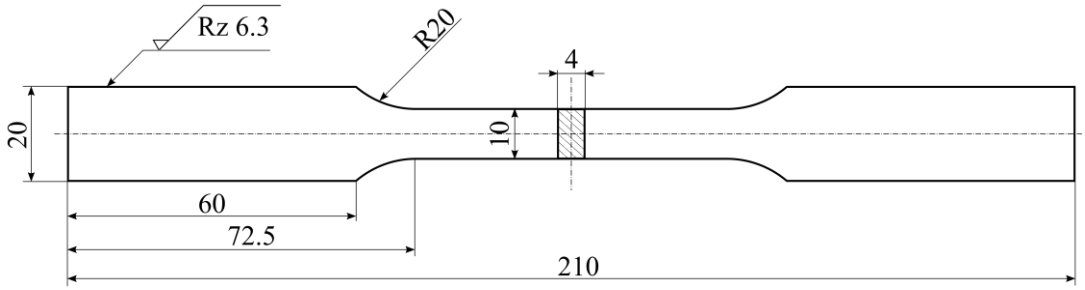

Figure 6. Specimen for the tensile tests

2.2.6. Statistical analysis and regression. The software Matlab was used to derive a multiple linear regression model, which describes the correlation between the welding temperature T_S (input), the welding speed v_S (input), and the UTS R_m (output). The software tool provides sample functions to fit the model and determines the fit quality. Usually, polynomial models are used due to their simplicity. In this paper, the differences between the model and the experimental data from study 1 were defined as residuals. The differences between model and experimental data from study 2 were defined as the prediction error, because the data from study 2 were not employed for modelling. During the fitting step, the coefficients of the polynomial were adjusted to minimize the mean squared error *MSE* of the residuals [17]. The model quality was assessed by employing the coefficient of determination R^2 [18]. The root mean squared error *RMSE* and the mean absolute error *MAE* are statistical measures that are used in this paper to quantify the differences between experiment and the model [17]. The hypothesis posed in section 2.1 was tested by comparing the *RMSE* and the *MAE* of the residuals and the prediction error, respectively. The equations used to calculate the statistical measures are described in the appendix.

3. Results and discussion

3.1. UTS and regression.

The resulting UTS data of both studies are given in Tables A 1 and A 2. The difference between minimum and maximum was approximately 150 MPa. Various trials from study 1 were replicated: the parameters from experiments no. 1, 12, and 9 were repeated in trials no. 21, 18, and 14 and yielded relative standard deviations of 0.85 %, 1.85 %, and 0.27 %, respectively. The center point (experiment no. 30) of the full factorial sub-plan in study 2 was repeated in trial no. 38, and no. 39. The resulting standard deviation was 0.8 %. This demonstrates the high reproducibility of FSW, because the standard deviation of the UTS remains within the same magnitude, regardless of whether the specimens were obtained from two different plates welded with the same parameters or from the same plate. The lowest UTS values, which resulted from samples welded with parameters from the lower boundary of the parameter window 2, showed a high standard deviation. The same characteristic was observed for the sample welded at the highest temperature and at the highest welding speed. This indicates that the process limits were reached.

A comparison of the resulting UTS for both studies shows good agreement (see Figure 7). Figure 7 illustrates the UTS for different welding temperatures at a welding speed of 50 mm/min. The values obtained from study 1 are marked as blue circles, the values obtained from study 2 are marked as green asterisks. Furthermore, the mean rotational speeds required to achieve the welding temperatures are depicted. Figure 7 shows that the differences between the rotational speeds from study 1 and from study 2 increase with increasing welding temperature. In contrast, the differences in UTS for similar welding temperatures are small. The general trend of the UTS from study 1 agrees with the results from study 2. The only exception is the sample welded with T_S = 485 °C (experiment no. 40). The standard deviation of the rotational speed is not depicted because the rotational speed was adjusted by the controller to maintain the set welding temperature. Accordingly, the standard deviation represents the activity of the controller rather than variations in the results by identical process parameters.

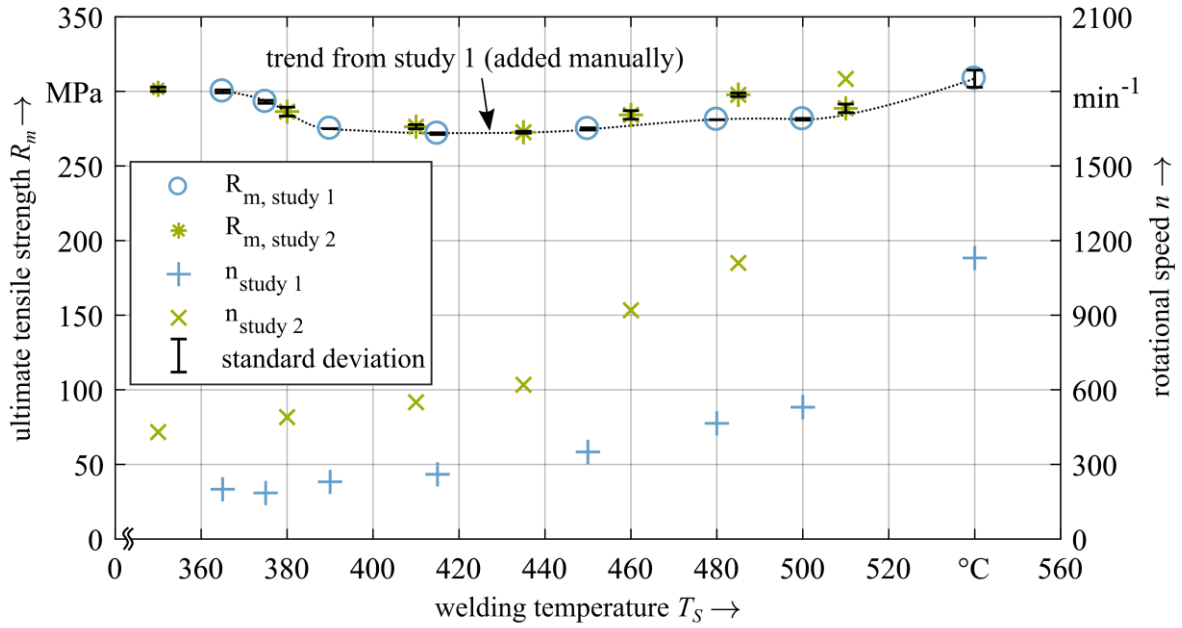

Figure 7. Mean ultimate tensile strength and mean rotational speeds for different welding temperatures at welding speed v_s = 50 mm/min

The data from study 1 were used to derive a regression model. The welding speed and the welding temperature were employed as input parameters, while the UTS served as the output parameter of the regression model. When multiple plates were welded with the same parameter sets the mean value was employed. In total 18 data sets were used to derive the model. A polynomial model of second order with

second order interactions provided the best fit quality. The model quality was quantified by the coefficient of determination R^2. A lower model order led to an insufficient model quality, while a higher order was assumed to result in overfitting. The polynomial of the identified model is:

$$R_m(T_S, v_s) = a_0 + a_1 \cdot v_S + a_2 \cdot T_S + a_3 \cdot v_S \cdot T_S + a_4 \cdot v_S \cdot T_S^2 + a_5 \cdot T_S^2 + a_6 \cdot v_S^2, \quad (1)$$

with the linear coefficients a_0, a_1, a_2 , a_3, a_4, a_5, and a_6. The coefficients of Eq. (1) as well as the coefficient of determination R^2 and the *RMSE* of the model residuals are given in Table 2. The p-values of the factors were smaller than 2 %. Consequently, all coefficients of Eq. (1) were determined to be significant [18].

Table 2. Model parameters

a_0 in MPa	a_1 in MPa·min^{-1}/mm	a_2 in MPa/°C	a_3 in MPa min^{-1} (mm·°C)	a_4 in MPa/(min^{-1}·°C^2)	a_5 in MPa/°C^2	a_6 in MPa·(min^{-2}/mm^2)	R^2	*RMSE* in MPa
1413.6	-7.1646	-5.0445	0.030386	$-3.0349 \cdot 10^{-5}$	$6.7401 \cdot 10^{-4}$	$5.4899 \cdot 10^{-3}$	0.98	3.71

The model was used to predict the UTS for the parameter sets of study 2. The absolute residuals and the absolute prediction errors are depicted in Figure 8. It can be observed that the prediction errors of the parameter sets of study 2, which were outside the parameter window of study 1 (i.e. no. 27, no. 28, no. 34, and no. 35), were significantly higher than those which were inside.

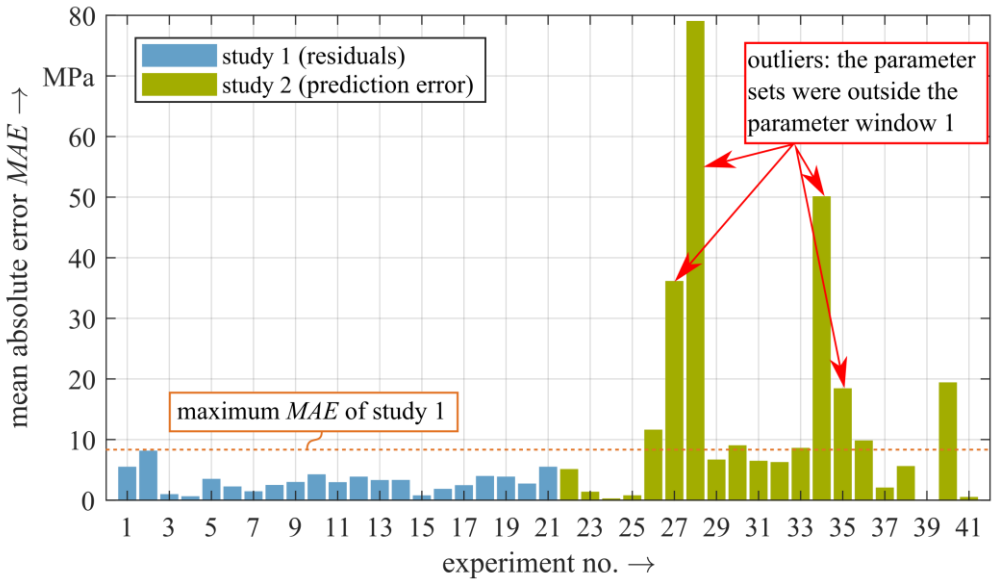

Figure 8. Mean absolute error (*MAE)* of both studies

Initially, the limited extrapolation capability of regression models was considered to be the reason for the high absolute prediction error. According to Table A 2, experiment no. 27 and no. 34 showed a relatively high standard deviation. This was interpreted as evidence of an unstable welding process. Hence, the cross-sections and the X-ray images were more intensely investigated. This revealed a tunnel defect on the advancing side in three parameter sets (i.e. no. 27, no. 34, and no. 35). The X-ray images of experiment no. 28 could not be interpreted clearly: it appeared as if the tunnel defect in the weld, which occurred at the parameter set no. 27, ceased in the transition zone of the plate. However, a reliable statement could not be made. Hence, the fractured surface of the tensile test specimens was analyzed. Thereby, a lack of consolidation was found on the advancing side of the weld.

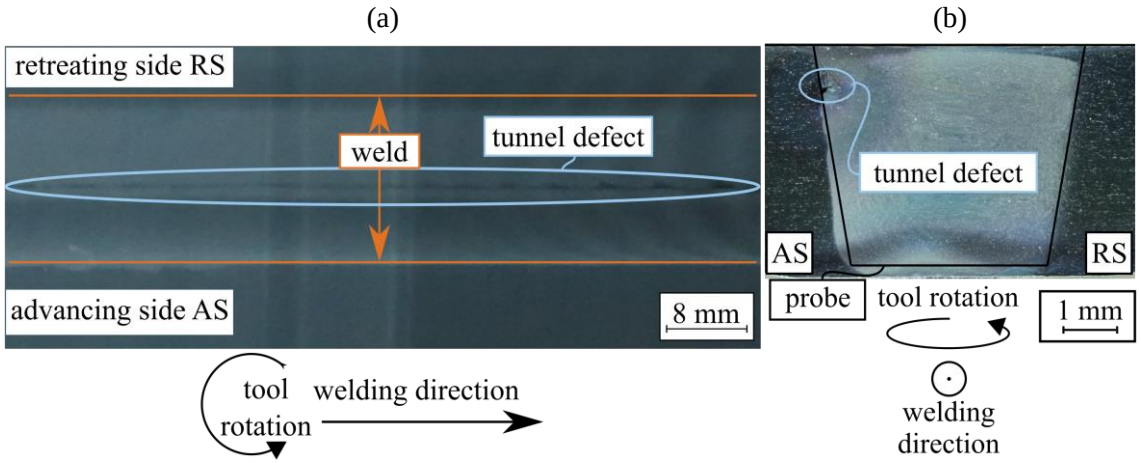

Figure 9. (a) X-ray image of the weld from experiment no. 34; (b) metallographic cross-section of the weld from experiment no. 34

Consequently, the results of experiments no. 27, no. 28, no. 34, and no. 35 were considered as outliers. The only remaining abnormality was experiment no. 40. It showed a relatively high not explainable prediction error. Therefore, the data from experiment no. 40 was included in the subsequent statistical analysis, whereas the outliers were considered separately.

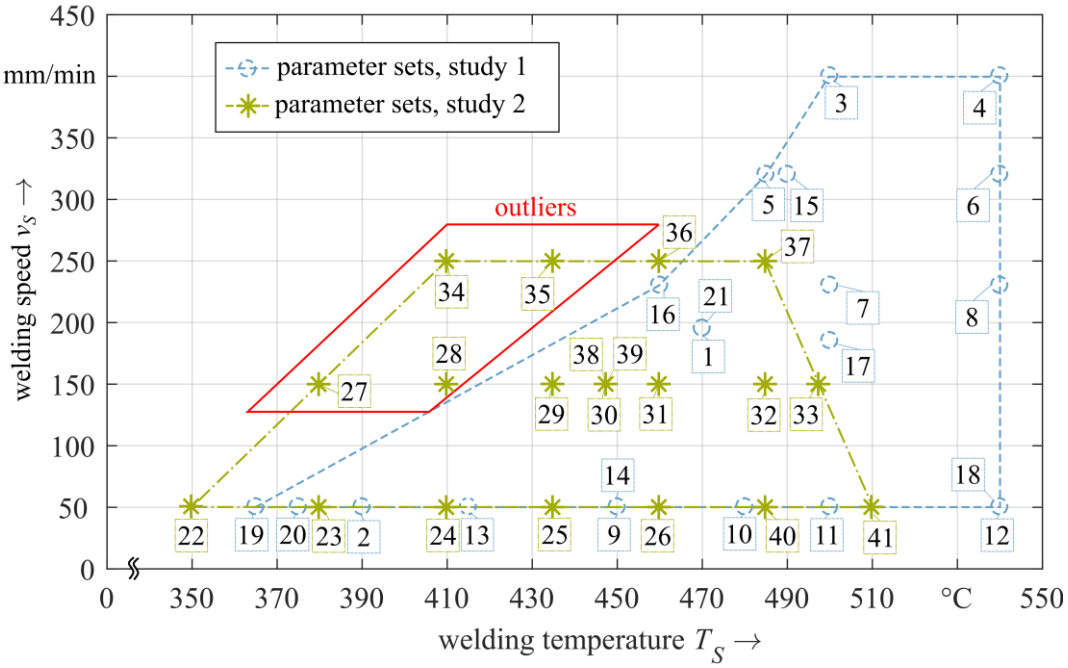

Figure 10. Parameter sets of study 1 and study 2 with identified outliers

The *RMSE* and the *MAE* for the prediction error as well as for the residuals are given in Table 3. Both measures of the prediction error without outliers are in the same range as the residuals. This means that the model describes the correlation between welding temperature, welding speed, and UTS of the weld accurately at a mean absolute prediction error of 6.03 MPa within the boundaries of the parameter window 1. The model is valid also for study 2, although a different tool size, a different downward force, and a different batch of raw material was used. The applicability of the model to a different experimental set-up leads to the conclusion that the relevant process parameters were identified. This means that the welding temperature und the welding speed are the determining factors for the UTS of friction stir welds in EN AW-2219-T87. This corroborates the hypothesis posed in section 2.1 and implies that a required

UTS can be ensured by maintaining an adequate welding temperature and welding speed. Furthermore, the results depicted in Figure 8 suggest that the rotational speed *n* does not influence the UTS directly. The results indicate that the rotational speed primarily serves as a heat source. The metallurgical effects, which occur during the welding process, are most likely caused by the thermal cycle and must therefore depend on temperature and time.

Table 3. *RMSE* and *MAE* calculated with the residuals and the prediction error

RMSE of the residuals in MPa	*MAE* of the residuals in MPa	*RMSE* of the prediction error with outliers in MPa	*MAE* of the prediction error with outliers in MPa	*RMSE* of the prediction error without outliers in MPa	*MAE* of the prediction error without outliers in MPa
3.710	3.430	23.81	13.99	7.720	6.030

4. Conclusions

Two parameter studies were conducted in order to investigate the influence of the welding temperature and the welding speed on the UTS of friction stir welds in EN AW-2219-T87. The results were used to derive a regression model, which describes the correlation between the two welding parameters and the UTS. This led to the following conclusions:

- The UTS of friction stir welds in EN AW-2219-T87 is determined predominantly by the welding temperature and the welding speed.
- The rotational speed primarily influences the welding temperature. The results suggest that the thermal cycle plays an important role for the UTS of the welds. It could be shown that samples joined using similar welding speeds and welding temperatures show similar UTS values, even though a significantly different rotational speed was employed.

The underlying effects, which cause the variance in the UTS, will be the subject of future investigations.

5. Appendices

The mean square error was determined according to

$$MSE = \frac{1}{n}\sum_{i=1}^{n}\left(R_{m,model,i} - R_{m,experiment,i}\right)^2, \tag{2}$$

with the UTS calculated by the model $R_{m,model}$, the UTS obtained from the experiment $R_{m,experiment}$, the total number of experimental points *n*, and the index variable *i* [17]. The coefficient of determination R^2 was calculated by

$$R^2 = 1 - \frac{\sum_{i=1}^{n}\left(R_{m,model,i} - R_{m,experiment,i}\right)^2}{\sum_{i=1}^{n}\left(R_{m,experiment,i} - \bar{R}_{m,experiment}\right)^2}, \tag{3}$$

with the mean value of the UTS $\bar{R}_{m,experiment}$ from the experiments. The mean value of the UTS was obtained by

$$\bar{R}_{m,experiment} = \frac{1}{n}\sum_{i=1}^{n} R_{m,experiment,i}. \tag{4}$$

The RMSE can be determined by the root of the MSE as follows:

$$RMSE = \sqrt{MSE} = \sqrt{\frac{1}{n}\sum_{i=1}^{n}\left(R_{m,model,i} - R_{m,experiment,i}\right)^2}. \tag{5}$$

The MAE was calculated by

$$MAE = \frac{\sum_{i=1}^{n} \Delta R_{m,abs,i}}{n}, \tag{6}$$

where

$$\Delta R_{m,abs,i} = \left| R_{m,model,i} - R_{m,experiment,i} \right|. \tag{7}$$

Table A 1. Experimental plan of parameter study 1

Exp. no.	Welding temperature T_S in °C	Welding speed v_S in mm/min	Mean rotational speed n in min^{-1}	Downward force F_z in N	Tilt angle β in °	Tool type -	Mean UTS R_m in MPa	Standard deviation of the UTS S_{Rm} in MPa
1	470	195	530	9000	2.5	1	315.67	4.16
2	390	50	230	9000	2.5	1	275.00	0.00
3	500	400	965	9000	2.5	1	333.33	5.51
4	540	400	1608	9000	2.5	1	339.67	14.43
5	490	320	835	9000	2.5	1	331.67	0.58
6	540	320	1510	9000	2.5	1	349.67	0.58
7	500	230	795	9000	2.5	1	331.00	1.00
8	540	230	1385	9000	2.5	1	343.00	1.00
9	450	50	350	9000	2.5	1	274.67	0.58
10	480	50	465	9000	2.5	1	281.00	0.00
11	500	50	530	9000	2.5	1	281.33	0.58
12	540	50	1100	9000	2.5	1	304.67	1.15
13	415	50	260	9000	2.5	1	271.67	0.58
14	450	50	356	9000	2.5	1	275.00	1.00
15	485	320	750	9000	2.5	1	324.75	1.00
16	460	230	600	9000	2.5	1	307.33	4.62
17	500	185	700	9000	2.5	1	320.00	1.00
18	540	50	1160	9000	2.5	1	312.33	6.03
19	365	50	200	9000	2.5	1	300.00	1.00
20	375	50	185	9000	2.5	1	293.00	1.00
21	470	195	530	9000	2.5	1	315.67	0.58

Table A 2. Experimental plan of parameter study 2

Exp. no.	Welding temperature T_S in °C	Welding speed v_S in mm/min	Mean rotational speed n in min^{-1}	Downward force F_z in N	Tilt angle β in °	Tool type -	Mean UTS R_m in MPa	Standard deviation of the UTS S_{Rm} in MPa
22	350	50	430	7000	2.5	2	301.46	1.15
23	380	50	490	7000	2.5	2	286.43	3.00
24	410	50	550	7000	2.5	2	276.31	1.39
25	435	50	620	7000	2.5	2	272.61	0.65
26	460	50	920	7000	2.5	2	284.20	2.87
27	380	150	650	7000	2.5	2	238.15	12.12
28	410	150	760	7000	2.5	2	202.86	5.48
29	435	150	960	7000	2.5	2	296.08	1.28
30	447,5	150	1020	7000	2.5	2	302.70	2.01
31	460	150	1080	7000	2.5	2	304.69	1.63
32	485	150	1470	7000	2.5	2	314.46	3.28
33	497,5	150	1670	7000	2.5	2	322.24	0.29
34	410	250	1000	7000	2.5	2	224.04	25.60
35	435	250	1180	7000	2.5	2	275.21	3.06
36	460	250	1680	7000	2.5	2	320.20	5.54
37	485	250	1810	7000	2.5	2	322.71	5.65
38	447,5	150	1030	7000	2.5	2	299.27	0.43
39	447,5	150	1030	7000	2.5	2	297.72	1.21
40	485	50	1110	7000	2.5	2	297.76	1.2
41	510	50	1850	7000	2.5	2	288.64	2.87

Table A 3. Tensile tests to characterize the base material

Specimen	UTS R_m in MPa
Base material in rolling direction	476
Base material perpendicular to the rolling direction	471
Base material perpendicular to the rolling direction	469

6. References

[1] Ostermann F 2014 *Anwendungstechnologie Aluminium (‚Application technology of Aluminum'),* (Berlin, Heidelberg: Springer)

[2] Colligan K J 2010 The Friction Stir Welding Process *Friction stir welding,* ed D Lohwasser and Z Chen (Cambridge, UK: Woodhead Publishing Limited) pp 15 – 41

[3] Kahnert M, Mestek M, Windisch M, Tessier I and Okualla M 2012 Preparation of Friction Stir Welding of the Aluminum Alloy AA 2219 for Launcher Applications *9th International Friction Stir Welding Symposium* (Huntsville, Alabama) May 15th–17th 2012

[4] Cao G and Kou S 2005 Friction Stir Welding of 2219 Aluminum: Behavior of (AI2Cu) particles *Welding Journal* **84** 1–7

[5] Elangovan K and Balasubramanian V 2007 Influences of pin profile and rotational speed of the tool on the formation of friction stir processing zone in AA2219 aluminium alloy *Materials Science and Engineering* A **459** 7–18

[6] Elangovan K and Balasubramanian V 2008 Influences of tool pin profile and welding speed on the formation of friction stir processing zone in AA2219 aluminium alloy *Journal of Materials Processing Technology* **200** 163–75

[7] Surekha K, Murty B S and Prasad Rao K 2009 Effect of processing parameters on the corrosion behaviour of friction stir processed AA 2219 aluminum alloy *Solid State Sciences* **11** 907–17

[8] Srinivasan P B, Arora K S, Dietzel W, Pandey S and Schaper M K 2010 Characterisation of microstructure, mechanical properties and corrosion behaviour of an AA2219 friction stir weldment *Journal of Alloys and Compounds* **492** 631–37

[9] Arora K S, Pandey S, Schaper M and Kumar R 2010 Microstructure Evolution during Friction Stir Welding of Aluminum Alloy AA2219 *Journal of Materials Science and Technology* **26** 747–53

[10] Schneider J, Stromberg R, Schilling P, Cao B, Zhou W, Morfa J and Myers O 2013 Processing effects on the friction stir weld stir zone *Welding Journal* **92** 11s–9s

[11] Doude H, Schneider J, Patton B, Stafford S, Waters T and Varner C 2015 Optimizing weld quality of a friction stir welded aluminum alloy *Journal of Materials Processing Technology* **222** 188–96

[12] Rao C V, Reddy G M and Rao K S 2015 Influence of tool pin profile on microstructure and corrosion behaviour of AA2219 Al–Cu alloy friction stir weld nuggets *Defence Technology* **11** 197–208

[13] Kang J, Feng Z-C, Frankel G.S, Huang I W, Wang G-Q and Wu Ai-Ping 2016 Friction Stir Welding of Al Alloy 2219-T8 *Metallurgical and Materials Transactions* A **47** 4553–65

[14] Kang J, Feng Z-C, Li J-C, Frankel G S, Wang G-Q amd Wu Ai-Ping 2016 Friction Stir Welding of Al Alloy 2219-T8 *Metallurgical and Materials Transactions* A **47** 4566–77

[15] Bachmann A, Gamper J, Krutzlinger M, Zens A and Zaeh M F 2017 Adaptive model-based temperature control in friction stir welding *The International Journal of Advanced Manufacturing Technology* **93** 1157–71

[16] Costanzi G, Bachmann A and Zaeh M. F 2017 Entwicklung eines FSW-Spezialwerkzeugs zur Messung der Schweißtemperatur (‚Development of a FSW tool to measure the Welding Temperature') *DVS Berichte vol 337* (Düsseldorf: DVS Media GmbH) 2017 119–125

[17] Kosfeld R, Eckey H F and Tuerck M 2016 *Deskriptive Statistik* (‚*Descriptive statistics*'), (Wiesbaden: Springer)

[18] Siebertz K, van Bebber D and Hochkirchen T 2010 *Statistische Versuchsplanung* (*‚Design of Experiments'*), (Heidelberg: Springer)

Acknowledgments

The IGF-research project no. 19.516 N of the "Research Association on Welding and Allied Processes of the DVS" has been funded by the AiF within the framework for the promotion of industrial community research (IGF) of the Federal Ministry for Economic Affairs and Energy because of a decision of the German Bundestag.
The authors would like to thank the German Research Foundation (DFG) for funding the project "Temperature Control in FSW". Additional gratitude is given to Amanda Zens, Manuel Kessler, and Philippe Schua for their assistance.